PCCP

Accepted Manuscript

ROYAL SOCIETY OF CHEMISTRY

www.rsc.org/pccp

Physical Chemistry Chemical Physics
CREATED USING THE RSC LaTeX PCCP ARTICLE TEMPLATE – SEE www.rsc.org/electronicfiles FOR DETAILS
ARTICLE TYPE www. rsc.org/xxxxxx | XXXXXXXX

Interaction of H_2O and H_2S with Cu(111) and the Impact of the Electric Field: Rotating & Translating Adsorbate, and Rippled Surface

Jin Hyun Chang,[a] Ahmed Huzayyin,[a,b] Keryn Lian,[c] and Francis Dawson[a]

Received Xth XXXXXXXXXX 20XX, Accepted Xth XXXXXXXXX 20XX
First published on the web Xth XXXXXXXXXX 200X
DOI: 10.1039/b000000x

The interactions of H_2O and H_2S monomers with Cu(111) in the absence and presence of an external electric field are studied using density functional theory. It is found that the adsorption accompanies a rippled pattern of the surface Cu atoms and an electron accumulation on the surface Cu atoms surrounding the adsorption site. The response of the H_2O/Cu(111) and H_2S/Cu(111) interfaces to the external electric field is computed up to the field magnitude of 10^{10} V/m. The results show that H_2O rotates and translates much more with an electric field than H_2S does. The extent of the surface deformation changes considerably with the applied electric field, which influences the translation pattern of the adsorbates. On the other hand, the rotation of the adsorbates is correlated to the dipole moment of the molecules and their adsorption energies.

1 Introduction

Understanding the nature of the interaction between the electrode and adsorbates is of great importance in many fields of applied science and engineering. Several relevant applications include corrosion prevention, hydrogen production and electrocatalytic energy conversion. However, understanding the physics of the interface on an atomic or electronic scale remains to be a challenging task [1–3]. One of the primary sources of the challenge is the presence of a high electric field at the interface. The electric field magnitudes reach in the order of 10^{10} V/m when a voltage is applied or current is injected into the electrode [1].

The interaction between monomers and the electrode in the presence of an external electric field is directly linked to many technological processes involving electrocatalytic reactions [4–7]. The monomeric adsorption of water-like molecules is difficult to characterize experimentally due to their tendency to form clusters [2,8]. Consequently, the characterization of monomer–electrode interactions that specifically includes the impact of the electric field relies on computational studies [1]. However, a comprehensive understanding of the behaviour of the interface in the presence of an external field is a major goal yet to be achieved [3].

We have recently investigated the nature of the interaction between a water monomer and gold electrodes, Au(111) and Au(110), with and without an external electric field using density functional theory (DFT) [9]. The Au–H_2O interaction was explained in terms of the interplay between covalent binding and electrostatic interactions. The covalent binding involves the interaction between the Au atoms, mainly their d orbital, with a $1b_1$ orbital (associated with the lone pair orbitals of the O atom) and the $3a_1$ orbital (attributed to orbitals of both O and H atoms) of the water monomer. These were respectively referred to as Au–O and Au–OH interactions. The electrostatic interaction is due to the interaction of the water dipole with the surface and the imposed electric field. The correlation between the adsorption angle and the contribution of Au–O and Au–OH interactions was also determined, where the adsorption angle α represents a vertical angle between the plane parallel to the electrode surface and a vector connecting O and H as shown in Fig. 1. The Au–O interaction was found to play a greater role in the overall water–electrode interaction than the Au–OH interaction for the molecule in a flat orientation ($|\alpha|$ is small) compared to the molecule in a vertical orientation ($|\alpha|$ is large) and vice versa.

The analysis of the adsorption of the water monomer on Au(111) and Au(110) [9] further showed that the covalent interaction between the water monomer and the gold surface is the dominant type of interaction in the absence of an electric field whereas the electrostatic interaction dominates at higher electric fields. When the electrostatic interaction becomes comparable to the covalent interaction, the H_2O molecule begins to rotate and its dipole orientation asymptotically approaches an alignment oriented in the direction of the electric field.

[a] *The Edward S. Rogers Sr. Department of Electrical & Computer Engineering, University of Toronto, 10 Kings College Road, Toronto, Canada. E-mail: jin.chang@mail.utoronto.ca*
[b] *Electrical Power & Machines Department, Cairo University, Giza, Egypt*
[c] *Department of Materials Science & Engineering, University of Toronto, 184 College Street, Toronto, Canada.*

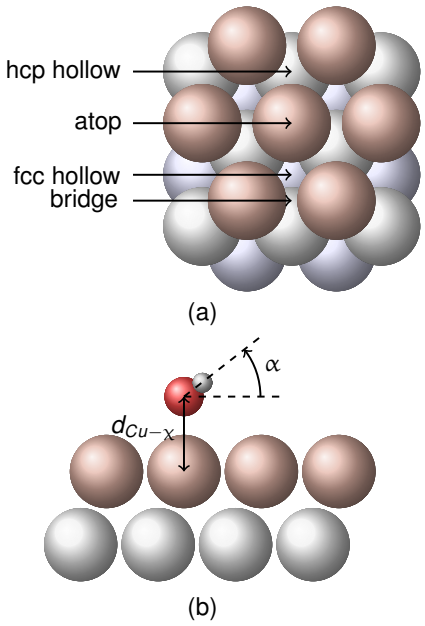

Fig. 1 Names of adsorption sites (a) and illustrations of adsorption angle and distance (b).

The present work aims to extend the understanding of the adsorbate–electrode interaction by investigating different electrode and adsorbate pairs using DFT. A copper electrode with (111) surface, Cu(111), was selected for the electrode because it has a similar electronic structure to that of gold but displays significantly different interfacial characteristics such as chemical reactivity and mechanical rigidity. In particular, the gold electrodes remained structurally insensitive to adsorption and the applied electric field[9]. The lack of a large structural change of the gold surfaces aligns well with the comparison made by Michaelides[10] where gold was one of the least structurally sensitive metals to water adsorption among the following matals: Ru, Rh, Pd, Pt, Cu, Ag and Au. Copper, on the other hand, was the most structurally sensitive metal to the adsorption of H_2O[10]. By analyzing the monomeric adsorption on Cu(111), one can assess not only the applicability of the aforementioned characteristics of H_2O/Au, but also the contribution of the surface structure change to the overall behaviour of the adsorbate/electrode interface.

On the adsorbate side, hydrogen sulfide was investigated in addition to the water monomer because it has the same number of lone pairs as water, is similar in size and structure, and has a different dipole moment compared to water as shown in Table 1. Particularly, the lone-pair orbital is known to contribute the most to the overall adsorbate–electrode interaction for both water and hydrogen sulfide[8,11] and the number of lone pairs of the two are the same. On the other hand, the dipole moments of the two molecules differ significantly (1.850 D for H_2O and 0.970 D for H_2S). The dipole moment is expected to play an increasing role when an electric field is applied. The dipole–field interaction is the greatest contributor to the electrostatic interaction in the presence of the electric field and it increases as the magnitude of the electric field increases[9].

Table 1 Comparison of H_2O and H_2S

	H_2O	H_2S
bond length (Å)	0.9572[12]	1.328[13]
bond angle (deg)	104.52[12]	92.2[13]
no. of lone pairs	2	2
dipole moment	1.850[14]	0.970[14]

A prime application of H_2O/Cu(111) is hydrogen production using a water gas shift reaction where a copper-based catalyst is widely used[15,16]. On the other hand, understanding the interaction between H_2S and copper is important in making copper-base catalysts: H_2S is a common impurity which promotes the formation of an S overlayer[11,17]. The tarnishing of copper also involves the H_2S/Cu interaction associated with the copper sulfidation process[18]. There are many other technological applications that can benefit from gaining further insights into the interaction between H_2O/H_2S and copper.

The magnitude of the electric field is increased in 10^9 V/m increments, in both positive and negative directions, with a maximum electric field magnitude of 10^{10} V/m. The responses of the adsorbates to the external field, namely rotation, translation and structural changes, are compared and linked to the nature of the adsorption without an external field. We demonstrate that the response of the adsorbate is nonlinear and asymmetric with respect to the magnitude and direction of the electric field and is influenced by the structural sensitivity of the electrode surface to the adsorption. The rotation of the adsorbates can be predicted from the dipole moment of the molecule and its adsorption energy. The adsorption of H_2O and H_2S accompanies a rippled pattern of the surface Cu atoms and the extent of the surface deformation needs to be considered to describe the translation pattern of the adsorbates. The rippled pattern of the surface atoms and its impact on the response of the interface to the external electric field have not been observed previously and are reported for the first time.

2 Computational Methods

The results presented in this work are based on DFT computations using the Quantum ESPRESSO package[19], which uses plane wave basis sets and applies periodic boundary conditions. The Perdew-Burke-Ernzerhof[20] exchange-correlation functional was used with the projector augmented wave type[21] pseudopotentials as constructed by Kresse and Joubert[22]. The

cutoff energy for wave functions and charge density were 70 Ry and 560 Ry, respectively. The surface was modelled using a $5 \times 3\sqrt{3}$ supercell, which corresponds to a 1/30 monolayer surface coverage. This structure is larger than any of the reported DFT investigations of Cu(111) and was chosen to avoid any artificial lateral interaction with its images created by periodic boundary conditions. The next section will show that a large lateral size of the supercell is critical in characterizing the electrode–adsorbate interaction both with and without the electric field. The slabs were separated by a vacuum greater than 20 Å to avoid the vertical interactions.

All of the results reported were computed using a slab consisting of 5 layers of Cu where the top 3 layers were fully relaxed while the bottom 2 layers were fixed at the bulk atomic coordinates, unless explicitly stated otherwise. Computations with a higher number of layers have been compared and the comparison confirmed the convergence and validity of the settings used. The dipole created by the lack of symmetry was compensated for by the insertion of the dipole layer in the middle of the vacuum[23], which was also used to introduce an external electric field. A Monkhorst-Pack type k-point grid[24] of $3 \times 3 \times 1$ was used for sampling the supercell. All of the values above were selected to ensure that the total energy converges within 0.01 eV. The validity of the DFT modeling approach was ensured by comparing parameters such as the bond lengths and angles of H_2O and H_2S, and the lattice constant of Cu and its work function to experimental values as shown in Table 2. The work function, Φ, was computed using the "bulk plus band line up" method[25]. The enthalpy of reaction, ΔH, corresponds to the change in the energy (or heat) accompanied by the reaction. The reactions are $H_2O \longrightarrow H_2 + \frac{1}{2}\,O_2$ for water and $H_2S \longrightarrow H_2 + \frac{1}{2}\,S_2$ for hydrogen sulfide. The enthalpy of reaction was computed as $\Delta H = \Delta E + \Delta ZPE$, where ΔE is the reaction energy and ΔZPE is the change in the zero-point energy (ZPE). E corresponds to the total electronic energy at ground state and it was computed by DFT via structural optimization to yield the minimum energy on the potential energy surface. The experimental values of ΔH were obtained by subtracting the sum of enthalpies of formation of reactants from the sum of the enthalpies of formation of products at 0 K. The values of the enthalpies of formation and ZPE are as reported in ref. 26. Given the expected level of accuracy of DFT (structural and energetic accuracies of around 3% and $10 \sim 20\%$[27], respectively), the agreement between computed values and those from experiment is satisfactory.

Table 2 Physical parameter values of molecules and electrode

Species	Parameter	Computed	Exp.	% error
H_2O	d_{H-O} (Å)	0.9724	0.9572[12]	1.6
	∠HOH (deg)	104.57	104.52[12]	0.05[a]
	ΔH (eV)	2.82	2.48[26]	13.7
H_2S	d_{H-S} (Å)	1.349	1.328[13]	1.6
	∠HSH (deg)	92.1	92.2[13]	0.1[a]
	ΔH (eV)	1.04	0.85[26]	23.0
Cu	a_o (Å)	3.671	3.610[28]	1.7
	Φ (eV)	4.81	4.98[29]	3.4

[a] in degrees

3 Results & Discussion

3.1 Adsorption without an Electric Field

It is known that the atop site (Fig. 1a) is the most stable adsorption site for both H_2O[10] and H_2S[30] on Cu(111) and other face-centered cubic (fcc) (111) surfaces. Therefore, only an atop site is considered for the adsorption for both monomers since the monomers would preferentially be adsorbed on an atop site. The most stable adsorbed structures of the monomers are determined through structural optimization computations using various initial orientations of the monomers on the atop site. A comparison between the adsorbed structures and adsorption energies of H_2O and H_2S at the atop site determined in the present work and previous work by others[4,10,11,17,31–33] is shown in Table 3. E_{ads} is the adsorption energy in eV. α (Fig. 1b), the adsorption angle, represents a vertical angle between the plane parallel to the electrode surface and a vector connecting the atom "χ" (the symbol χ stands for O in the case of water and S in the case of hydrogen sulfide) and H. α is defined so that a positive angle corresponds to a "hydrogen-up" orientation while a negative angle corresponds to a "hydrogen-down" orientation. $d_{Cu-\chi}$ (Fig. 1b) represents the distance between χ and the surface Cu atom that is immediately underneath the adsorbate. The lateral size of the supercell used for the results is shown in terms of the effective surface coverage (Θ) of the water.

Table 3 Adsorbed structure and energy in the absence of the external electric field

Adsorbate	Source	E_{ads} (eV)	α (deg)	$d_{Cu-\chi}$ (Å)	Θ (ML)
H_2O	this work	−0.19	19.89	2.32	1/30
	Ref. 31[a]	−0.18	20.8	2.33	1/20
	Ref. 4	−0.21	7	2.34	1/9
	Ref. 32	−0.24	3	2.40	1/9
	Ref. 10	−0.24	15	2.25	1/4
	Ref. 33	−0.19[b]	8.7	2.36	1/4
H_2S	this work	−0.25	14.00	2.46	1/30
	Ref. 11	−0.23	13	2.51	1/9
	Ref. 17	−0.28	13.6	2.41	1/9

[a] Authors used multiple cell sizes for a comparison. The results with the largest cell size is shown here. [b] Originally reported in kJ/mol and converted to eV.

It is known that the modelling parameters such as a size of the cell and effective surface coverage influence the computation results[34,35]. The lateral size of the cell is particularly important in studying the adsorption of polar molecules[35]. Considering the large variations in the lateral sizes of the cells used for the results shown in Table 3, the results of this work show an acceptable agreement with other DFT computation results. It was previously mentioned that the lateral size of the cell in this work is larger than any of the reported results. The results are in much better agreement if we compare our results with that of the work employing the next largest lateral size[11,17,31]. In particular, the adsorption energy and geometry of water found in this work and by Nadler and Sanz[31] are almost the same. The remaining results show larger variations in both E_{ads} and the adsorption geometry due to the smaller lateral size of the cell.

It has been reported that the potential energy surface (PES) is relatively flat and as a result, small variations in water geometry (e.g., α and $d_{\mathrm{Cu}-\chi}$) have a little impact on E_{ads}[36]. This was also shown to be true when Nadler and Sanz[37] compared the impact of cell size on the adsorption of the water monomer on Au(111): different cell sizes cause the geometry of the water to change while E_{ads} remains insensitive. The difference in both the geometry and adsorption energy as the size of the cell is varied signals that the artificial interactions with the periodic images may be severe enough to distort the PES when the cell size is too small. The detailed analysis, to follow, shows that the adsorbate–electrode interaction spreads out laterally and involves multiple atoms of the electrode in the first two atomic layers from the surface.

The range of E_{ads} shows that the nature of adsorption for both H_2O and H_2S is weak chemisorption/physisorption. The adsorption angle is related to the relative strengths of the Cu–χ, Cu–Hχ and electrostatic interactions. The electrostatic interaction forces the orientation of the adsorbates to be in a vertical hydrogen-up orientation[9,10,36], i.e., $\alpha = 90^\circ$. The adsorption angles of 14.00° and 19.89°, both very far from the 90° imposed by electrostatic interaction, show that the electrostatic interaction is not the dominant type of interaction for both H_2O and H_2S. Instead, the covalent interaction is the strongest component of the overall interaction between the adsorbate and the electrode.

The relevant contributions of Cu–χ and Cu–Hχ interactions can be investigated by the projected density of states (PDOS) analysis, which projects density of states onto individual atoms (or orbitals of an atom). By projecting the DOS onto individual atoms, the contribution of each atom to the adsorption can be studied by comparing the PDOS of the molecules in isolated and adsorbed states. More changes of the PDOS (i.e., a shifting and broadening) means a greater contribution of the corresponding state, or orbital, to the adsorption process. The PDOS plots of H_2O/Cu(111) and H_2S/Cu(111) are shown in Fig. 2. To display the impact of adsorption, the PDOS of the adsorbates at isolated (left) and adsorbed (right) states are shown next to each other on the same scale. The energy is measured with respect to the vacuum level, E_{vac}. The dashed horizontal line represents the Fermi level and the shaded area represents the sum of the PDOS of the 3*d* orbitals of the surface Cu atoms. The cell size of 30 Å × 30 Å × 30 Å was used to compute the PDOS of the isolated molecules and E_{vac} was measured in the direction perpendicular to the direction of the dipole moment to eliminate its impact.

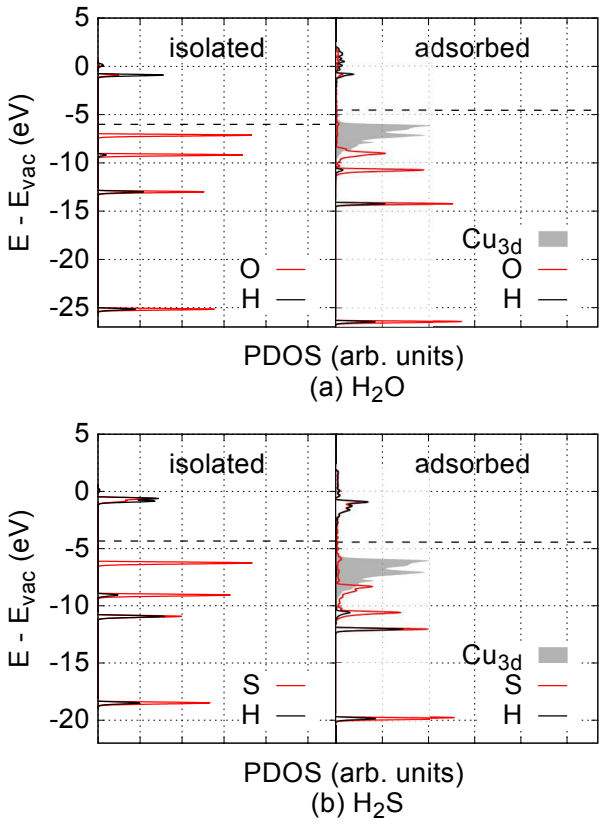

Fig. 2 PDOS of (a) H_2O and (b) H_2S in isolated (left) and adsorbed (right) settings. A different scale is used for the PDOS of 3*d* orbitals to increase the visibility of all of the PDOS.

For both H_2O and H_2S, the highest occupied molecular orbital (HOMO) is composed only of orbitals of χ atoms, commonly referred to as the lone-pair orbital. It can be seen from Fig. 2 that the lone-pair orbitals display the most significant interaction with the 3*d* orbitals of the surface Cu atoms and also the most change (e.g., peak PDOS value, energy shifting and broadening) upon adsorption compared to other states at lower energies. This reveals that the Cu–χ interaction is the strongest interaction for both H_2O and H_2S. The stronger Cu–χ interaction is in agreement with the prediction that a

small α value corresponds to a strong interaction between χ and the electrode[8–10,38]. Additionally, the PDOS change of the lone-pair orbitals is slightly greater for H_2S, suggesting that the Cu–χ interaction is stronger for H_2S than for H_2O. Based on the fact that the Cu–χ interaction is the most dominant type of interaction for adsorption, the stronger E_{ads} and larger $d_{Cu-\chi}$ of H_2S compared to that of H_2O can be explained by differences between the $2p$ orbital of O and the $3p$ orbital of S atoms. The $3p$ orbital spreads out further in space compared to the $2p$ orbital with a peak of the electron probability distribution radially farther away from its nucleus. This allows more overlap between the $3p$ and Cu(111) surface orbitals. Consequently, lone-pair orbitals of H_2S mix more with the $3d$ orbital, which leads to a stronger adsorption at a larger equilibrium distance.

The states below the HOMO are formed by orbitals of both H and χ atoms, and the changes of these states can be linked to the Cu–Hχ interaction. A comparison of the changes of the PDOS of the energy state below the HOMO shows that the Cu-Hχ interaction is stronger for H_2S than for H_2O. The stronger Cu–S and Cu–HS interactions compared to Cu–O and Cu–HO interactions mean that H_2S adsorbs more strongly to the Cu(111) surface than H_2O does, which is consistent with the higher E_{ads} of H_2S ($E_{ads} = -0.25$ eV for H_2S and $E_{ads} = -0.19$ eV for H_2O).

Another means of investigating the nature of the interaction is to perform a difference charge density, $\Delta\rho$, analysis. The $\Delta\rho$ plot is shown in Fig. 3. $\Delta\rho$ can be found by subtracting the charge densities of the clean electrode and isolated adsorbate from the charge density of the adsorbate–electrode interface, i.e., $\Delta\rho = \rho_{ads/\mathrm{Cu}(111)} - \rho_{ads} - \rho_{\mathrm{Cu}(111)}$. The $\Delta\rho$ analysis allows one to understand the charge transfer (both the extent of the transfer and the participating atoms) when the adsorbate and electrode are interacting. In Fig. 3, the red isosurface represents an accumulation of charge and the blue isosurface represents a depletion of charge. The figure shows that most of the charge transfer occurs between the adsorbate and the region between the adsorbate and the surface layer, similar to the results found for a water bilayer on Pt(111)[39] and Ru(0001)[40]. Therefore, the term "charge rearrangement" is more appropriate than the term "charge transfer" between the adsorbate and the electrode. A key feature of the charge rearrangement is a depletion of charge in the region between the adsorbate and the Cu atom underneath it (Cu_1) and an accumulation of charge around the six surrounding surface Cu atoms which form a hexagonal ring (Cu_6). This observation implies an interesting feature of the adsorption of $H_2\chi$ on Cu(111): the adsorption of $H_2\chi$ affects Cu_1 and Cu_6 in an opposite manner. A further analysis and discussion will follow on this observation.

To validate the observations based on Fig. 3, the structural changes of the surface Cu atoms are also analyzed. Table 4 shows the translations of the Cu atom below the adsorbate

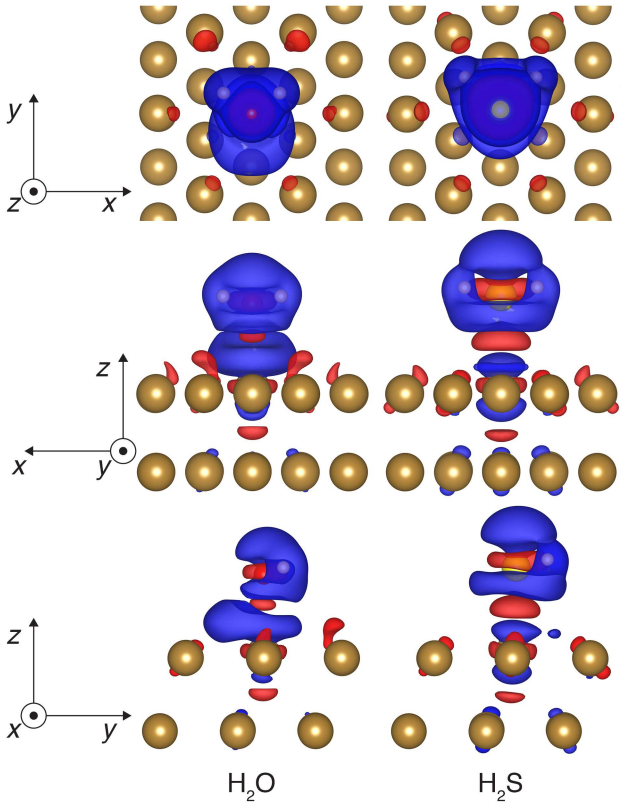

Fig. 3 Charge density difference of H_2O/Cu(111) (left) and H_2S/Cu(111) (right). A blue (red) isosurface represent a depletion (accumulation) of charge.

(d_{Cu_1}) and the six Cu atoms forming a hexagonal ring (d_{Cu_6}) around the adsorbate. The direction of d_{Cu_1} is almost entirely upwards towards the adsorbate, while the direction of d_{Cu_6} is away from the adsorbates (i.e., laterally outwards and vertically downwards). A maximum (d_{Cu_6-max}), a minimum (d_{Cu_6-min}) and an average value (d_{Cu_6-avg}) of the translations of the six Cu atoms are reported for d_{Cu_6}. The directions of the translation would suggest that there is an attractive force between $H_2\chi$ and Cu_1 and a repulsive force between $H_2\chi$ and Cu_6. The greater extent of the translation in the case of H_2S adsorption compared to H_2O adsorption agrees with the stronger adsorption of H_2S indicated by the PDOS analysis and E_{ads}.

Table 4 Translation of surface copper atoms upon adsorption

Adsorbate	d_{Cu_1} (Å)	d_{Cu_6-avg} (Å)	d_{Cu_6-min} (Å)	d_{Cu_6-max} (Å)
H_2O	0.081	0.024	0.022	0.026
H_2S	0.155	0.028	0.025	0.032

Although an attractive force exists between the adsorbate

and the Cu atom underneath, one cannot determine the source of the translation of the six surface Cu atoms based on the translation and charge redistribution pattern. It could be either due to the repulsive interaction with the adsorbate, or simply due to the upshift of the Cu atom in the middle of the ring. To further investigate the source of this translation, structure optimization computations were performed without the adsorbate while the Cu_1 atom was fixed at the upshifted position. The top three layers except for Cu_1 were allowed to move freely. The results show that the six Cu atoms translated almost entirely upwards by 0.011 Å ($d_{Cu_6-avg} = 0.011$ Å, $d_{Cu_6-max} = 0.012$ Å $d_{Cu_6-min} = 0.010$ Å) when $d_{Cu_1} = 0.081$ Å, and by 0.014 Å ($d_{Cu_6-avg} = 0.014$ Å, $d_{Cu_6-max} = 0.015$ Å $d_{Cu_6-min} = 0.014$ Å) when $d_{Cu_1} = 0.155$ Å. This shows that the upshift of the Cu_1 atom brings the six surrounding Cu atoms with it, causing them to translate in the same upwards direction.

An additional set of the structure optimization computations was carried out to validate the presence of the repulsive type interaction. $H_2\chi$ was adsorbed to the surface while the Cu_1 atom was fixed at its original position while the remaining Cu atoms in the top three layers and $H_2\chi$ were fully relaxed. This time, the six Cu atoms translated away from the adsorbate by 0.020 Å ($d_{Cu_6-avg} = 0.020$ Å, $d_{Cu_6-max} = 0.022$ Å $d_{Cu_6-min} = 0.018$ Å) when H_2O was adsorbed, and by 0.041 Å ($d_{Cu_6-avg} = 0.041$ Å, $d_{Cu_6-max} = 0.047$ Å $d_{Cu_6-min} = 0.034$ Å) when H_2S was adsorbed. Therefore, it can be seen that the interaction between $H_2\chi$ and Cu_6 shows a repulsive characteristic. However, it is important to stress that one cannot be sure if the repulsive characteristic is a result of a direct repulsive force between $H_2\chi$ and Cu_6. It is also possible that the presence of $H_2\chi$ causes the charge to be accumulated around the six Cu atoms (a red isosurface in Fig. 3), which causes the six Cu atoms to repel each other. In either case, the presence of $H_2\chi$ causes the six Cu atoms to move away from the adsorbate and it is not due to the upshift of the Cu atom in the middle of the ring.

One way to explain the nature of the observed attractive/repulsive pattern is by using a "*d*-band model"[41,42], which describes the interaction between an adsorbate and a transition metal surface. According to the *d*-band model, the adsorption energy is greater if a greater extent of the *d*-band of the metal is filled (i.e., a larger fraction of the *d*-band is below the Fermi level). This correlation is related to the mobility of *d*-electrons which move away from the adsorption site to reduce the Pauli repulsion: *d*-electrons move more (less) freely to reduce the Pauli repulsion if the *d*-band is less (more) populated. For the case of copper, a nearly fully occupied *d*-band (d^{10}) makes the *d*-electrons immobile, which makes Cu(111) hydrophobic. This also agrees well with the weak adsorption energies of $H_2\chi$. However, much more mobile *sp*-electrons move away from the adsorption site to reduce the Pauli repulsion. Using this concept, Schiros *et al.*[43] explained the different water wetting behaviour of Cu(110) compared to Cu(111). They found that although the electronic structure (filled *d*-band) is the same for Cu(110) and Cu(111), Cu(110) is hydrophilic because it is geometrically corrugated and *sp*-electrons preferentially occupy the region between Cu atoms[43], which leaves the adsorption site electron deficient.

A possible scenario that describes the adsorption process which causes the rippled surface pattern is deduced based on the *d*-model and mobile *sp*-electrons of copper. When $H_2\chi$ is adsorbed, the mobile *sp*-electron of the Cu_1 atom moves out laterally along the surface to Cu_6 atoms to minimize the Pauli repulsion force. This facilitates the adsorption of $H_2\chi$ by making the Cu_1 atom electron deficient which helps it to share the electrons with $H_2\chi$. The sharing of the electron (i.e., dative bond) involves an attraction force and thus, $H_2\chi$ pulls the Cu_1 atom upwards. The Cu_6 atoms with the excess *sp*-electron (which will preferentially move towards the surface of Cu or a space between Cu_1 and Cu_6) repel each other and thus, move away from $H_2\chi$. This description matches well with the observed pattern and is also consistent with the conventional understanding that the adsorbed water (and hydrogen sulfide for this work) acts as an electron donor and the electron deficient atop site acts as an electron acceptor[44]. The main difference from the conventional picture is that the excess electron from $H_2\chi$ is not localized to the adsorption site, but is spread across Cu_6.

The observed charge redistribution and structural changes of the surface Cu atoms indicate that the adsorbate–electrode interaction spreads out laterally on the surface. This lateral interaction sets a lower bound on the surface size and thus, the supercell of different surface sizes are compared with varying levels of structural relaxations. The surface sizes compared are shown in Fig. 4. The surface sizes of $2 \times \sqrt{3}$, $4 \times 2\sqrt{3}$ and $5 \times 3\sqrt{3}$ correspond to a 1/4, 1/16 and 1/30 monolayer surface coverage, respectively. The surface coverage is measured in terms of the ratio between the number of adsorbates and the number of surface atoms (e.g., 1 monolayer corresponds to the presence of one adsorbate – H_2O or H_2S – for every surface Cu atom). It is emphasized that a significant artificial interaction with the periodic images is expected for a $2 \times \sqrt{3}$ supercell and is included for a comparison. Each of the surface sizes are computed with a water monomer adsorbed at the atop site while 0, 1, 2 and 3 top layers of the electrode are relaxed. For $4 \times 2\sqrt{3}$ and $5 \times 3\sqrt{3}$, the results obtained when only the underlying Cu atom is relaxed (Cu_1) and when the underlying Cu atom and six surrounding Cu atoms are relaxed (Cu_7) are also compared. A comparison of the computation results is shown in Table 5. The H_2O/Cu(111) interface is discussed to demonstrate the impact of the surface size of the supercell and the number of relaxed atoms/layers. The same trend is expected

for H_2S/Cu(111) as it shares similar interaction characteristics (i.e., charge redistribution and structural changes).

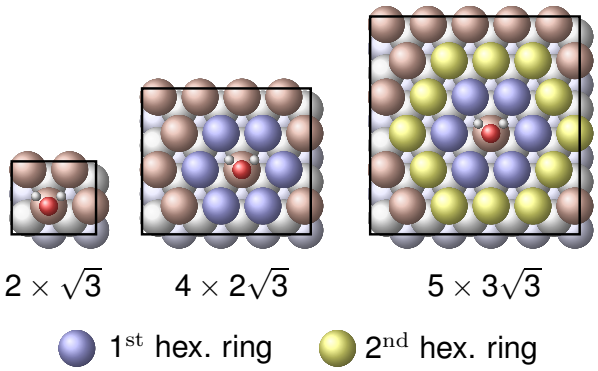

Fig. 4 Sizes of surface compared and the hexagonal rings included.

Table 5 Adsorption geometry and energy of H_2O/Cu(111) with various surface sizes and structural relaxation levels in the absence of the external electric field

Size	relaxed layer	E_{ads} (eV)	α (deg)	d_{Cu-O} (Å)	d_{Cu_1} (Å)	d_{Cu_6-avg} (Å)
$2\times\sqrt{3}$	0	−0.15	−0.14	2.61	···	···
	1	−0.16	0.43	2.52	0.063	···
	2	−0.17	2.00	2.52	0.059	···
	3	−0.17	1.94	2.51	0.044	···
$4\times2\sqrt{3}$	0	−0.17	17.11	2.43	···	···
	Cu_1	−0.17	16.83	2.37	0.069	···
	Cu_7	−0.18	17.74	2.36	0.065	0.022
	1	−0.18	17.84	2.36	0.067	0.023
	2	−0.19	16.26	2.34	0.094	0.023
	3	−0.19	17.13	2.34	0.093	0.023
$5\times3\sqrt{3}$	0	−0.17	18.54	2.42	···	···
	Cu_1	−0.18	20.18	2.35	0.073	···
	Cu_7	−0.18	20.46	2.35	0.066	0.020
	1	−0.19	19.84	2.35	0.071	0.019
	2	−0.19	19.35	2.32	0.098	0.020
	3	−0.19	19.89	2.32	0.081	0.024

The comparison of the three surface sizes shows that both the adsorption energy and geometry obtained using a $2\times\sqrt{3}$ supercell differs significantly from the results obtained using larger cells. This confirms that the lateral size corresponding to the effective surface coverage of 1/4 ML is too small to introduce a significant artificial interaction with its periodic images. The differences between the $4\times2\sqrt{3}$ and $5\times3\sqrt{3}$ supercells show that the adsorption geometry is more sensitive to the lateral size change than E_{ads}, which agrees with the previous DFT studies on 4*d* metal surfaces [36,37]. Additionally, the greater α and smaller d_{Cu-O} pattern for a larger surface supercell shows that the O atom gets closer to the surface with an increased surface size while H atoms remain relatively fixed in height. The increased adsorption strength with a greater level of relaxation and lateral size indicates that the structural changes of the copper electrode facilitates the adsorption of $H_2\chi$.

Both $4\times2\sqrt{3}$ and $5\times3\sqrt{3}$ surface sizes include the hexagonal ring formed by six Cu atoms. However, the latter includes the secondary hexagonal ring which surrounds the first hexagonal ring as shown in Fig. 4. This additional ring acts as a "cushion" where it reduces the interaction of the six Cu atoms in the first ring with the periodic images of the H_2O. Although the impact of inclusion of the second hexagonal ring is not as severe as the inclusion of the first ring, both adsorption geometry and adsorption energy show changes, following the same pattern when the first ring is included. It is believed that a further reduction in the lateral size from the $4\times2\sqrt{3}$ supercell will lead to the computation results that deviate more from that obtained using the $5\times3\sqrt{3}$ supercell. This is also indicated by a large variation in adsorption geometry and energy in the comparison shown in Table 3, even for the cases where a first hexagonal ring is included ($\Theta = 1/9$). The impact of the relaxed layers is also compared. The contribution of the level of relaxation is significant up to the top two layers, but a further relaxation does not alter the computation results considerably.

It should be noted that the lower bound of the surface supercell size and the number of relaxed layer varies from one type of metal to another. The vertical translations of the atom underneath the adsorbed H_2O are reported for several types of metal surfaces such as Ru(0001), Rh(111), Pd(111), Pt(111), Cu(111), Ag(111) and Au(111) by Michaelides *et al.* [10]. The comparison was made using 2×2 supercell and thus, the direction and magnitude of the translation of the surrounding Cu atoms are missing. However, the comparison showed that Cu(111) displays the largest structural changes among the types of surfaces they investigated. This suggests that Cu(111) is structurally more sensitive to the adsorption than the metal surfaces considered in ref. 10, which means that other types of metal surfaces may be less influenced by the supercell size. Lastly, it can be seen from Table 3 that the rippled structure of Cu(111) increases the adsorption energy by around 0.02 eV. Although its contribution is small, the presence of the water molecules in the neighboring adsorption sites (e.g., a water bilayer structure which takes a hexagonal arrangement [35]) interrupts the rippled pattern which may reduce the adsorption strength of the water molecule. This may contribute to the hydrophobic nature of Cu(111) surface where the water does not form a bilayer structure but instead forms 3D clusters [2,45,46]. However, further investigation is needed to determine the impact of the rippled surface on the wettability of the surface.

The reported results are based on Cu(111), but a similar type of interaction is expected for other transition metals to a varying extent. The fundamental understanding of the nature

of adsorption interaction and types of forces that exist are becoming increasingly more important, especially for the cases where multiple adsorbates are present and interact with another. For example, a repulsive force between the adsorbates has been recognized and recently been utilized to engineer a pattern of adsorbates on the surface or to control the extent of charge transfer between the adsorbate and surface (e.g., free-base porphine on Ag(111)[47], benzene and its derivatives on Cu(111)[48], etc.). Recently, the adsorbate–adsorbate interaction was taken into account in studying the electrocatalytic CO_2 reduction and it was shown to affect the catalytic activity[49]. In addition, the structural changes of the electrode surface, to be discussed in detail in the next section, is correlated to the translation of the adsorbates when an external electric field is applied to the interface. The rotation and translation of the adsorbate is of particular interest in energy storage and catalysis applications because it is directly linked to the electronic polarizability of the interface.

3.2 Impact of an External Electric Field

The characteristics of the adsorption of H_2O and H_2S to Cu(111) such as the adsorption energy and angle, the relative strengths of the Cu–χ interaction, the surface deformation and charge redistribution have been discussed in the absence of the external electric field. These characteristics can be used to predict the response of the interfaces when they are exposed to an external electric field. This section discusses the computation results in the presence of the external electric field and which information from the previous analysis (i.e., in the absence of the electric field) is relevant in predicting the response of the interface to the electric field.

A normal external electric field is applied to both H_2O/Cu(111) and H_2S/Cu(111) up to $\pm 1 \times 10^{10}$ V/m with a $\pm 1 \times 10^{9}$ V/m increment. The sign of the electric field is positive when the direction of the field is directed outwards from the surface, which corresponds to the direction of the electric field when the surface is positively charged. The adsorption angle, α, of both adsorbates is shown with respect to the external electric field in Fig. 5a. The orientation of both H_2O and H_2S becomes more hydrogen-up and hydrogen-down with the positive and negative electric field, respectively. It can also be seen that the rotation of H_2O is more sensitive to the external electric field than H_2S, which remains rigid without much rotation. The rotation of H_2O also shows that it is asymmetric with respect to the direction of the electric field – it is more sensitive to a negative electric field. The asymmetry and greater rotation for a negative electric field agrees with the previously observed pattern for a water molecule adsorbed on gold[9] and copper[32] electrodes.

The difference in the rotation of the two adsorbates can be explained/predicted by two parameters that are closely linked to the degree to which the adsorbates respond to the external electric field. The first parameter is the adsorption energy, E_{ads}, which is the energy that binds the adsorbate to the electrode. A higher E_{ads} means that the adsorbate is bound strongly to the surface via covalent interactions between the adsorbate and Cu atoms of the electrode. The relative contribution of the Cu–χ and Cu–Hχ interactions to E_{ads} changes as the orientation of the adsorbate is varied[8] and thus, E_{ads} is used as a parameter to describe the adsorbate–electrode interaction. As discussed above, a significant contribution of the overall adsorbate–electrode interaction comes from the Cu atoms that are not directly underneath the adsorbate. The interaction with multiple Cu atoms indicates that the higher E_{ads} is linked to how strongly the adsorbate is "locked" in the original orientation.

The second parameter is the dipole moment of the adsorbate. In the absence of an external field, the covalent interaction dominates over the electrostatic interaction, which is a dipole–dipole interaction between the adsorbate and its image in the electrode. When the external electric field is applied, a dipole–field interaction is introduced and its strength increases with the higher electric field. While the electric field is the control parameter, the dipole moment is the characteristic of the molecule itself and remains relatively constant. Therefore, it is expected that a higher E_{ads} and lower dipole moment of an adsorbate lead to an electrode/adsorbate interface that is less sensitive to the external field and vice versa.

H_2S has a higher E_{ads} and a lower dipole moment compared to H_2O, both of which make H_2S less responsive to the external electric field compared to H_2O. In other words, H_2S requires a higher electric field compared to H_2O in order to make a complete rotation ($\alpha = \pm 90^\circ$). This description matches well with the large difference in $\Delta\alpha$ in Fig. 5a. The inertness of H_2S is not only observed in the small change in α, but also in the change in the bond angle of the adsorbate as shown in Fig. 5b: the range of observed bond angle for H_2O is around 4° while the bond angle of H_2S remains virtually unchanged. The asymmetry and higher sensitivity to a negative electric field is again observed for the bond angle change for H_2O. The electrostatic energy due to the external electric field is determined by computing the difference in E_{ads} with and without the field while all of the atoms are fixed at their relaxed locations (in the presence of the field). The difference in E_{ads} corresponds to the electrostatic energy due to the field. The electrostatic energy due to $E = +1 \times 10^{9}$ V/m is 13.3 % and 8.7 % of E_{ads} for H_2O and H_2S, respectively, indicating that the field alters the adsorption characteristics of H_2O more significantly.

The rotations of H_2O and H_2S can also be explained with the electrostatic model of Maschhoff and Cowin[50]. According to the model, the total energy acting to rotate the adsorbate from a flat to a complete hydrogen-up orientation is written as

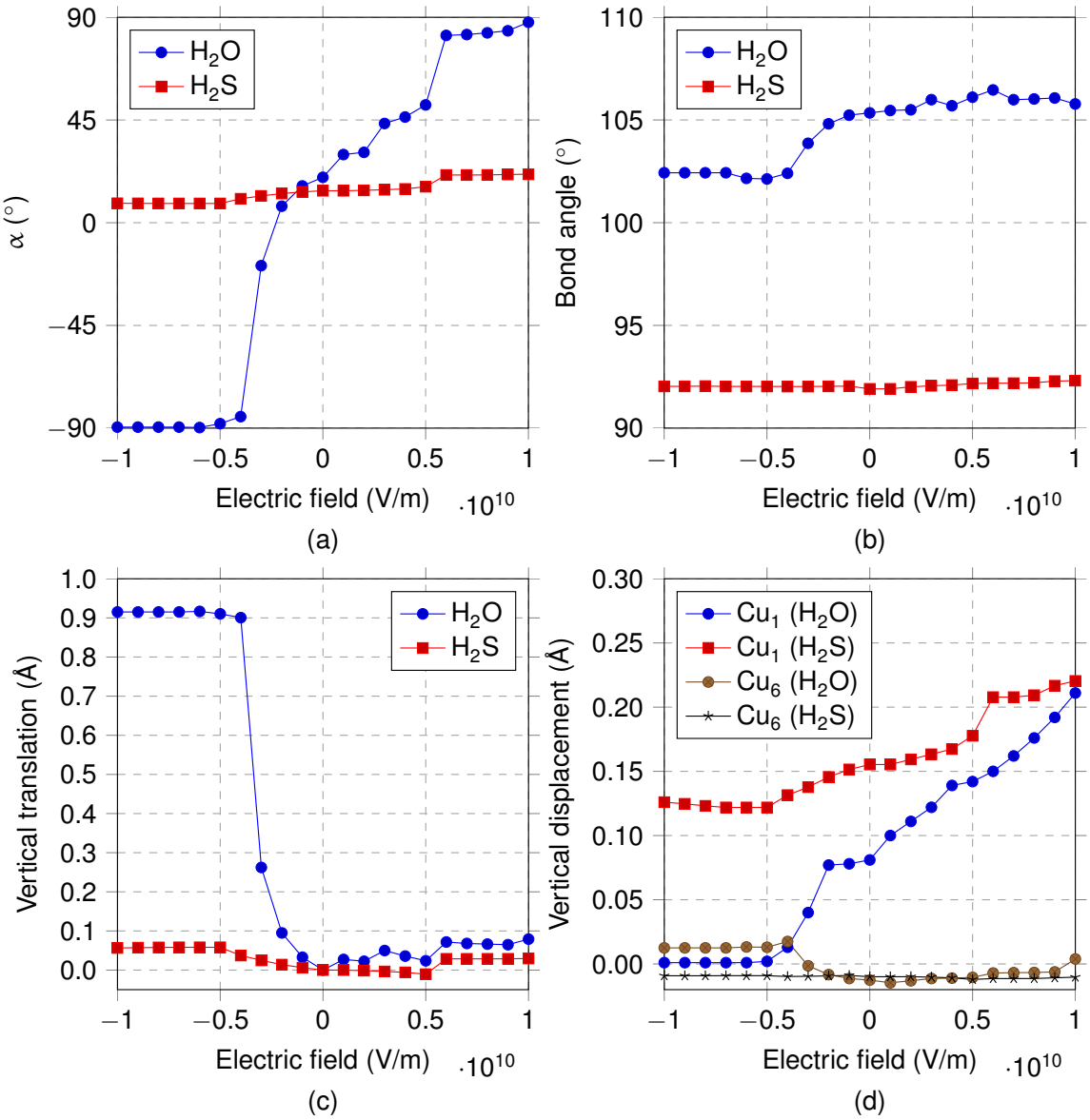

Fig. 5 Change in (a) adsorption angle, (b) bond angle, (c) vertical translation of the adsorbates and (d) vertical displacement of Cu_1 and Cu_6 with respect to the normal external electric field. An average value is used for the vertical displacement of Cu_6.

$U = -\frac{1}{2}\mu_0 E$. U, μ_0 and E are the total energy of the dipole, dipole moment of the adsorbate and magnitude of the external electric field, respectively. At high electric field values, the polarization energy and dipole image energy can be neglected for simplicity. Using the expression above, the electrostatic energy acting to rotate H_2O and H_2S from a flat to a complete hydrogen-up position is -0.19 eV and -0.10 eV at $E = +1 \times 10^{10}$ V/m, respectively. This energy is about the same as the the adsorption energy of H_2O and thus can rotate water to a hydrogen-up orientation, which is consistent with our observation. On the other hand, the electrostatic energy of -0.10 eV for H_2S at $E = +1 \times 10^{10}$ V/m is far smaller than its adsorption energy of -0.25 eV, which agrees with the predicted small rotation.

The vertical translations of H_2O and H_2S are shown in Fig. 5c, where the centres of mass in the absence of the external electric field is used as a reference point to measure the translation. A positive and negative translation corresponds to the adsorbate moving away and towards the electrode, respectively. Similar to the rotation, H_2S remains less sensitive to

the electric field than H_2O and the adsorbates translate more in response to a negative field compared to the positive electric field. Except for few small positive electric field values where the translation of H_2S is slightly downwards, the translation is upwards for both negative and positive electric fields. This pattern contrasts with what is reported for H_2O/Au [9] where the translation is towards the surface for positive electric fields while it is away from the surface for negative electric fields. Another difference from the H_2O/Au case is that the magnitude of the translation for H_2O/Cu is almost twice for a negative field and half for a positive electric field compared to H_2O/Au. These differences, both in direction and magnitude, are related to the structural changes of the copper surface, which is greater for copper compared to gold.

The vertical displacements of Cu_1 and Cu_6 with respect to the external electric field are shown in Fig. 5d, where the displacement is measured with respect to their original positions prior to the adsorption. The average value of the six Cu atoms are used for measuring the displacement of Cu_6. Similar to the structural changes of the adsorbates, the extent of the surface deformation also changes as the external field is applied. It can be seen that (i) there is a significant vertical translation of Cu_1 and the direction of the translation of Cu_1 is downward for a negative electric field and upward for a positive electric field.

The translation pattern of the adsorbates and the underlying Cu atoms (Fig. 5c and Fig. 5d) reveals some interesting features of the interface under the influence of an external electric field. Firstly, when the negative electric field is applied, the adsorbates not only rotate to become more hydrogen-down, but they also move away from the electrode. The vertical translations of both adsorbate and the underlying Cu atom can be explained by the fact that the rotation of the adsorbates reduces the originally dominant Cu–χ interaction as O and S atoms face away from the interacting Cu electrode. As a consequence, the attraction force between Cu_1 and the adsorbate becomes weaker, causing the adsorbates to move away from the surface while Cu_1 approaches its original position in the absence of the adsorbates. The weaker interaction between H_2O and Cu(111) at strong negative electric fields coincides with the more mobile H_2O molecule on Cu(111) when the electrode is negatively charge as suggested by Zhang *et al.* [32]. However, the change in the binding strength is expected to be much less for H_2S/Cu(111) at negative electric fields.

An opposite trend is shown when a positive electric field is applied: the rotation makes O and S atoms face toward the surface. Although the positive vertical translation of the adsorbates is observed for most of the points, it can be seen from Fig. 5d that the vertical translation of the underlying Cu atom is greater in magnitude. This shows that the distance between the adsorbate and the underlying Cu atom decreases as the magnitude of the positive electric field increases. It is difficult to determine definitively whether the adsorbates move towards or away from the surface when the positive electric field is applied because the surface becomes further deformed from its original flat structure. However, the decreased distance between $H_2\chi$ and Cu_1 suggests that the binding strength between the adsorbates and Cu_1 is greater when a positive electric field is applied. No considerable change is observed for H_2S/Cu(111), except that the Cu(111) surface is further deformed.

The translation of the adsorbates for H_2O/Cu(111) and H_2S/Cu(111) differs significantly from the case of H_2O/Au both in magnitude and direction. The difference is related to the structural sensitivity of the electrode surfaces to the presence of the adsorbates and electric field. For H_2O/Au, the water molecule is mainly responsible for the geometric response of the interface to the electric field where H_2O moves towards and away from the surface when positive and negative electric fields are applied, respectively. On the other hand, the structural changes of the Cu surface contribute significantly to the translation of the H_2O/Cu(111) interface. The Cu surface plays an even larger role in the response of the H_2S/Cu(111) interface, where the translation of the Cu_1 atom is comparable to the translation of the H_2S molecule. Therefore, the surface structure of the electrode needs to be included in the analysis of the $H_2\chi$/Cu(111) interface both in the absence and presence of the electric field, unlike most of the reported studies of metal/adsorbate systems.

4 Conclusions

The investigation suggests that the interaction between the lone pair orbitals of the adsorbates and the electrode is the largest contributor to the overall adsorption interaction although the role of Cu–Hχ interaction cannot be neglected. The $\Delta\rho$ profile and the structural changes show that a considerable part of the overall adsorbate–electrode interaction is attributed to the interaction with the six surrounding surface Cu atoms that form a hexagonal ring structure. The adsorption of $H_2\chi$ attracts the underlying Cu atom towards the adsorbate while the six surrounding Cu atoms move away from it. The presence of the mixed attractive and repulsive behaviour of the adsorbates could have a major implication in understanding the adsorbate–adsorbate interaction, which is becoming increasingly more important. The interaction between $H_2\chi$ and electrode penetrates two layers below the electrode surface and spreads out laterally. This requires a large lateral size for the supercell to accurately describe the $H_2\chi$/Cu(111) interaction.

When an external electric field is applied, the dipole–field interaction increases the electrostatic energy and the molecule starts to rotate to become more hydrogen-up oriented for positive electric fields and hydrogen-down oriented for negative

electric fields. The computation results show that a higher adsorption energy and lower dipole moment lead to an interface that responds more sensitively to the external electric field. However, it is found that for the case of Cu(111), the structural changes of the electrode surface need to be considered in order to understand the translation behaviour of the adsorbate. Therefore, the adsorption energy, dipole moment of the adsorbates and the structural sensitivity of the electrode surface (i.e., extent of deformation of the surface structure upon the adsorption of molecules and presence of the electric field) are the main parameters that are linked to how the interface reacts to the electric field. This relationship may serve as a stepping-stone towards developing a complete framework for the interaction of H_2O and similar molecules on transition metal electrodes in the presence and absence of an external electric field. The applicability of the observed trends to interfaces consisting of other transition metals and the water-like molecules requires further investigations.

The most prominent difference in the behaviour of H_2O and H_2S on Cu(111) is in their response to an electric field. H_2S remains rigid with a very small rotation and translation for a range of normal external electric fields up to $\pm 1 \times 10^{10}$ V/m. The structural changes of the electrode surface are comparable to that of the geometric changes of H_2S. On the other hand, H_2O undergoes a near complete rotation and significant translation. This means that the relative behaviour of H_2O/Cu(111) and H_2S/Cu(111) such as the binding energy and mobility of the adsorbates along the surface can be easily tuned by simply charging the Cu electrode. The findings of this work can be applied to systems where H_2O and H_2S coexist, such as a water gas shift reaction on Cu(111)[6].

5 Acknowledgement

The authors thank the support by the NSERC CREATE Program. Computations were performed on the gpc supercomputer at the SciNet HPC Consortium. SciNet is funded by: the Canada Foundation for Innovation under the auspices of Compute Canada; the Government of Ontario; Ontario Research Fund - Research Excellence; and the University of Toronto.[51]

References

1 E. M. Stuve, *Chem. Phys. Lett.*, 2012, **519–520**, 1–17.
2 J. Carrasco, A. Hodgson and A. Michaelides, *Nat. Mater.*, 2012, **11**, 667–674.
3 J. Rossmeisl, E. Skúlason, M. E. Bjorketun, V. Tripković and J. K. Nørskov, *Chem. Phys. Lett.*, 2008, **466**, 68–71.
4 A. A. Phatak, W. N. Delgass, F. H. Ribeiro and W. F. Schneider, *Journal of Physical Chemistry C*, 2009, **113**, 7269–7276.
5 J. Ren and S. Meng, *Journal of the Electrochemical Society*, 2008, **77**, 054110.
6 C. Callaghan, I. Fishtik, R. Datta, M. Carpenter, M. Chmielewski and A. Lugo, *Surface Science*, 2003, **541**, 21–30.
7 Y. Santiago-Rodríguez, J. A. Herron, M. C. Curet-Arana and M. Mavrikakis, *Surface Science*, 2014, **627**, 57–69.
8 A. Michaelides, *Appl. Phys. A: Mater. Sci. Process.*, 2006, **85**, 415–425.
9 A. Huzayyin, J. H. Chang, K. Lian and F. Dawson, *J. Phys. Chem. C*, 2014, **118**, 3459–3470.
10 A. Michaelides, V. Ranea, P. de Andres and D. King, *Phys. Rev. Lett.*, 2003, **90**, 216102.
11 P. N. Abufager, P. G. Lustemberg, C. Crespos and H. F. Busnengo, *Langmuir*, 2008, **24**, 14022–14026.
12 W. S. Benedict, N. Gailar and E. K. Plyler, *J. Chem. Phys.*, 1956, **24**, 1139–1165.
13 H. C. Allen, Jr and E. K. Plyler, *J. Chem. Phys.*, 1956, **25**, 1132–1136.
14 R. D. Nelson, Jr, D. R. Lide, Jr and A. A. Maryott, *Selected Values of Electric Dipole Moments for Molecules in the Gas Phase*, Natl. Stand. Ref. Data Ser. (U. S., Natl. Bur. Stand.), U.S. Government Printing Office: Washington, DC, 1967.
15 J. L. C. Fajín, F. Illas and J. R. B. Gomes, *J. Chem. Phys.*, 2009, **130**, 224702.
16 J. A. Rodriguez, J. C. Hanson, D. Stacchiola and S. D. Senanayake, *Phys Chem Chem Phys*, 2013, **15**, 12004.
17 Q.-L. Tang, S.-R. Zhang and Y.-P. Liang, *J. Phys. Chem. C*, 2012, **116**, 20321–20331.
18 T. T. M. Tran, C. Fiaud and E. M. M. Sutter, *Corros. Sci.*, 2005, **47**, 1724–1737.
19 P. Giannozzi, S. Baroni, N. Bonini, M. Calandra, R. Car, C. Cavazzoni, D. Ceresoli, G. L. Chiarotti, M. Cococcioni, I. Dabo, A. D. Corso, S. de Gironcoli, S. Fabris, G. Fratesi, R. Gebauer, U. Gerstmann, C. Gougoussis, A. Kokalj, M. Lazzeri, L. Martin-Samos, N. Marzari, F. Mauri, R. Mazzarello, S. Paolini, A. Pasquarello, L. Paulatto, C. Sbraccia, S. Scandolo, G. Sclauzero, A. P. Seitsonen, A. Smogunov, P. Umari and R. M. Wentzcovitch, *J. Phys.: Condens. Matter*, 2009, **21**, 395502.
20 J. P. Perdew, K. Burke and M. Ernzerhof, *Phys. Rev. Lett.*, 1996, **77**, 3865–3868.
21 P. E. Blöchl, *Phys. Rev. B*, 1994, **50**, 17953–17979.
22 G. Kresse and D. Joubert, *Phys. Rev. B*, 1999, **59**, 1758–1775.
23 J. Neugebauer and M. Scheffler, *Phys. Rev. B*, 1992, **46**, 16067–16080.
24 H. J. Monkhorst and J. D. Pack, *Phys. Rev. B*, 1976, **13**, 5188–5192.
25 R. Ramprasad, N. Shi and C. Tang, in *Dielectric Polymer Nanocomposites*, ed. J. K. Nelson, Springer US, 2010, ch. 5, pp. 133–161.
26 *NIST Chemistry WebBook, NIST Standard Reference Database Number 69*, ed. P. J. Linstrom and W. G. Mallard, National Institute of Standards and Technology, Gaithersburg MD, 20899, 2014.
27 W. Kohn, *Rev. Mod. Phys.*, 1999, **71**, 1253–1266.
28 N. W. Ashcroft and N. D. Mermin, *Solid State Physics*, Holt, Rinehart and Winston, New York, 1st edn., 1976.
29 H. B. Michaelson, *J. Appl. Phys.*, 1977, **48**, 4729–4733.
30 M. P. Hyman, B. T. Loveless and J. W. Medlin, *Surf. Sci.*, 2007, **601**, 5382–5393.
31 R. Nadler and J. F. Sanz, *J. Mol. Model.*, 2011, **18**, 2433–2442.
32 P. Zhang, W. T. Zheng and Q. Jiang, *Journal of Physical Chemistry C*, 2010, **114**, 19331–19337.
33 Q.-L. Tang and Z.-X. Chen, *Surface Science*, 2007, **601**, 954–964.
34 A. Groß, *Surface Science*, 2012, **606**, 690–691.
35 A. Poissier, S. Ganeshan and M. V. Fernández-Serra, *Phys Chem Chem Phys*, 2011, **13**, 3375.
36 J. Carrasco, A. Michaelides and M. Scheffler, *Journal of Chemical Physics*, 2009, **130**, 184707.
37 R. Nadler and J. F. Sanz, *J. Chem. Phys.*, 2012, **137**, 114709.
38 V. Ranea, A. Michaelides, R. Ramírez, J. Vergés, P. de Andres and D. King, *Phys Rev B*, 2004, **69**, 205411.
39 S. Schnur and A. Groß, *New J. Phys.*, 2009, **11**, 125003.
40 G. Materzanini, G. Tantardini, P. Lindan and P. Saalfrank, *Phys. Rev. B*,

2005, **71**, 155414.
41 B. Hammer and J. K. Nørskov, *Nature*, 1995, **376**, 238–240.
42 B. Hammer and J. K. Nørskov, *Surface Science*, 1995, **343**, 211–220.
43 T. Schiros, O. Takahashi, K. J. Andersson, H. Öström, L. G. M. Pettersson, A. Nilsson and H. Ogasawara, *The Journal of Chemical Physics*, 2010, **132**, 094701.
44 P. A. Thiel and T. E. Madey, *Surf. Sci. Rep.*, 1987, **7**, 211–385.
45 M. Mehlhorn and K. Morgenstern, *Physical Review Letters*, 2007, **99**, 246101.
46 M. Meyer, J. Stähler, D. O. Kusmierek, M. Wolf and U. Bovensiepen, *Phys Chem Chem Phys*, 2008, **10**, 4932–4938.
47 F. Bischoff, K. Seufert, W. Auwärter, S. Joshi, S. Vijayaraghavan, D. Écija, K. Diller, A. C. Papageorgiou, S. Fischer, F. Allegretti, D. A. Duncan, F. Klappenberger, F. Blobner, R. Han and J. V. Barth, *ACS Nano*, 2013, **7**, 3139–3149.
48 S. Simpson and E. Zurek, *J. Phys. Chem. C*, 2012, **116**, 12636–12643.
49 C. Shi, H. A. Hansen, A. C. Lausche and J. K. Nørskov, *Phys Chem Chem Phys*, 2014, **16**, 4720–4727.
50 B. L. Maschhoff and J. P. Cowin, *Journal of Chemical Physics*, 1994, **101**, 8138.
51 C. Loken, D. Gruner, L. Groer, R. Peltier, N. Bunn, M. Craig, T. Henriques, J. Dempsey, C.-H. Yu, J. Chen, L. J. Dursi, J. Chong, S. Northrup, J. Pinto, N. Knecht and R. V. Zon, *J. Phys.: Conf. Ser.*, 2010, **256**, 012026.